Structure and spectroscopy of Pa^{4+} defects in Cs_2ZrCl_6. An *ab initio* theoretical study

Luis Seijo[a] and Zoila Barandiarán
Departamento de Química, C-XIV and Instituto Universitario de Ciencia de Materiales Nicolás Cabrera, Universidad Autónoma de Madrid, 28049 Madrid, Spain

(Received 25 May 2001; accepted 10 July 2001)

In this paper we present the results of spin–orbit relativistic *ab initio* model potential embedded cluster calculations on $(PaCl_6)^{2-}$ embedded in a reliable representation of the Cs_2ZrCl_6 host. Totally symmetric local distortions and vibrational frequencies are calculated for all the states of the $5f^1$ and $6d^1$ manifolds, as well as the corresponding $5f \leftrightarrow 6d$ transition energies and the shape of the $5f(\Gamma_{8u}) \leftarrow 6d(\Gamma_{8g})$ fluorescence band. An excellent overall agreement with available experimental data is observed which allows us to conclude that the quality of the spin–orbit operators used is very high for actinide elements, as was already known for transition metal and lanthanide elements. Furthermore, it is concluded that the structural and spectroscopic information produced here is very reliable and that the $6d(\Gamma'_{8g})$ state is around 10 000 cm^{-1} higher in energy than it was thought; our calculations suggest a value of 30 000 cm^{-1} for the $10Dq$ parameter of Pa^{4+} in Cs_2ZrCl_6, which would be compatible with the lower limit of 20 000 cm^{-1} accepted for Ce^{3+} in Cs_2NaYCl_6.
 [DOI: 10.1063/1.1398092]

I. INTRODUCTION

$5f \rightarrow 6d$ absorption and $6d \rightarrow 5f$ emission transitions have been observed in actinide ion impurities in ionic crystals.[1–4] Contrary to the case of $5f \rightarrow 5f$ transitions, they are often not well understood.[3,4] In effect, the $5f \rightarrow 5f$ transitions are identified with the help of the crystal field theory (CFT). In these systems the number of CFT parameters is very large, usually above 20, and they cannot be fitted to the experimental data without experiencing numerical problems. However, this shortcoming is often by-passed by fixing many of these parameters to reasonable values.[3] Trying to follow the same procedure for the $5f \rightarrow 6d$ transitions is usually impossible, due to the much larger number of CFT parameters. In consequence, the $5f \rightarrow 6d$ transitions are often unassigned. The contribution of *ab initio* calculations in this task can be of great help, provided that they include all the relevant effects: scalar and spin–orbit relativistic effects, electron correlation effects, and embedding effects. Recent *ab initio* calculations on the $5f$ manifold and on some charge transfer states of actinyl ions have been shown to be instrumental in the understanding of their electronic structure and spectra in solid state and in solution.[5–8]

Exceptionally, the $5f \rightarrow 6d$ transitions in Pa^{4+} impurities can be assigned because the open-shell configurations in the relevant states are $5f^1$ and $6d^1$, leading to simple CFT matrices lacking $5f-5f$, $6d-6d$, and $5f-6d$ electron repulsion parameters.[9] This fact makes the Pa^{4+} impurity especially interesting from the theoretical point of view because it provides a perfect case for the validation of the theoretical methods that can be applied later to impurities with a more complex electronic structure. The $5f \rightarrow 6d$ absorption spectrum and the $6d \rightarrow 5f$ emission spectrum of Pa^{4+}-doped Cs_2ZrCl_6 have been measured with high resolution and analyzed in great detail.[1,2] A problem remains, however, in the interpretation of the $6d^1$ states: The $6d$ crystal field splitting, 10Dq, of Cs_2ZrCl_6:Pa^{4+} is smaller than that of Ce^{3+} in Cs_2NaYCl_6, whereas the larger extension of the $6d$ orbitals of Pa^{4+} with respect to the $5d$ orbitals of Ce^{3+} would make one expect a larger d crystal field splitting.[2]

Among the theoretical methods able to calculate the structure and spectroscopy of actinide impurities in ionic crystals, the *ab initio* model potential method (AIMP)[10–12] has been shown to properly represent embedding effects in ionic hosts,[11,12] on the one hand, and scalar and spin–orbit relativistic effects in main group elements and transition elements such as Ni^{2+}-doped MgO,[13] Ir^{+} and Pt,[14,15] on the other hand. Recently, the relativistic core *ab initio* model potentials of the lanthanide and actinide elements based on Cowan–Griffin–Wood–Boring[16,17] atomic calculations have been published and their good performance in scalar relativistic effects has been pointed out.[18] Whereas the quality of the spin–orbit operators is good for the lanthanides,[19] it has not yet been tested for the actinide elements.

In this paper, we present the results of AIMP theoretical calculations on the local structure of Pa^{4+} impurities in the Cs_2ZrCl_6 host, in its ground- and low excited states with main character $5f^1$ and $6d^1$, and the corresponding absorption and emission transitions. Our goal is twofold: First, we want to test the performance of the AIMP method in the calculation of actinide $5f$ and $6d$ spin–orbit coupling splittings. Nowadays, these cannot be tested in atomic calculations because of the lack of experimental data in free actinide atoms and ions. The test in actinide ion impurities in ionic hosts demands a reliable representation of bonding and embedding effects, which could otherwise contaminate the results and make the analysis difficult. Second, we intend to

[a]Electronic mail: luis.seijo@uam.es

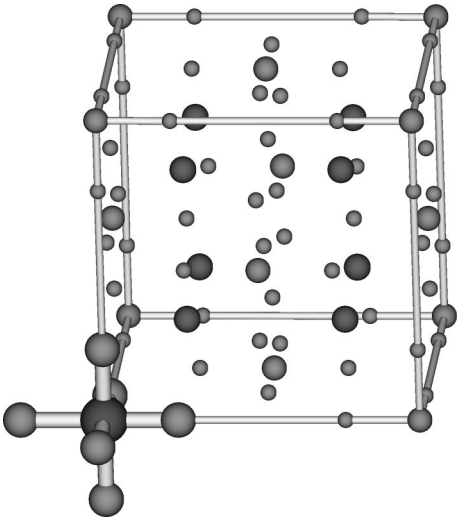

FIG. 1. Unit cell of Cs_2ZrCl_6 with a substitutional Pa^{4+} defect. The first coordination shell of six Cl^- ions with O_h symmetry has been enhanced. Nearest neighbors to the $(PaCl_6)^{2-}$ cluster are Cs^+ ions (111 directions) and $(ZrCl_6)^{2-}$ units (100, 010, 001 directions).

clarify the nature of the $6d^1$ excited states of Pa^{4+}-doped Cs_2ZrCl_6. In particular, we discuss the assignment of the upper $6d(\Gamma_8')$ state, which is responsible for the low value of $10Dq$, and we propose its change, as well as a considerably larger value of $10Dq$ which is coherent with that of Ce^{3+} in chloride hosts.

In Sec. II we present the details of the calculations and we discuss the results in Sec. III. The conclusions appear in Sec. IV.

II. METHOD AND DETAILS OF THE CALCULATIONS

The optical spectrum of Pa^{4+}-doped Cs_2ZrCl_6, where the Pa^{4+} impurities substitute for some of the Zr^{4+} ions in an O_h site, corresponds to electronic transitions localized in the unit $(PaCl_6)^{2-}$,[1] which are mainly influenced by all the atomic interactions within Pa^{4+} and by its bonding interactions with the first coordination shell of Cl^- ions (see Fig. 1.) Accordingly, we have performed wave function-based *ab initio* calculations on the $(PaCl_6)^{2-}$ defect cluster. These have been Hartree–Fock (SCF) and average coupled-pair functional (ACPF)[20] calculations including electron correlation effects. Since the relativistic effects in Pa^{4+} are very large and, in particular, the spin–orbit coupling dominates the nature of the manifold of states, we have used the Wood–Boring[17]-based effective core potential two-component relativistic Hamiltonian WB-AIMP.[12,21] Furthermore, the simultaneous inclusion of electron correlation effects and spin–orbit coupling is compulsory in this sytem but it is very demanding: We have used the two-step procedure based on the spin–free-state-shifted Hamiltonian (sfss)[12,13] in order to approximately decouple electron correlation and spin–orbit coupling effects and, so, largely simplify the calculations. All the details of the $(PaCl_6)^{2-}$ cluster are reported in Sec. II B. Finally, the embedding effects due to interaction of this cluster with the rest of the Cs_2ZrCl_6 host crystal have been included by means of the AIMP embedding technique;[11,12] the details are reported in Sec. II A. The calculations have been performed with the MOLCAS-5 package[22] and with a modified version of the COLUMBUS package.[23]

A. Embedding potential

The embedding potential that represents the effects of the Cs_2ZrCl_6 host on the $(PaCl_6)^{2-}$ defect cluster was obtained as described in Refs. 11 and 12. It is a one-electron effective potential that is added to the Hamiltonian of the otherwise isolated $(PaCl_6)^{2-}$ cluster. It results from the addition of total-ion *ab initio* model potentials (V_μ^{AIMP}) for all the ions in the crystalline lattice (μ:Cs^+, Zr^{4+}, and Cl^-),

$$V_{\mathrm{embedding}} = \sum_i \sum_\mu V_\mu^{\mathrm{AIMP}}(i), \tag{1}$$

with

$$V_\mu^{\mathrm{AIMP}}(i) = V_\mu^{lr-\mathrm{Coul}}(i) + V_\mu^{sr-\mathrm{Coul}}(i) + V_\mu^{\mathrm{Exch}}(i) + P_\mu(i). \tag{2}$$

Each total-ion potential is made of (1) a long-range Coulomb potential, which is a point-charge potential, so that $\Sigma_\mu V_\mu^{lr-\mathrm{Coul}}$ is the Madelung potential created by the host lattice within the cluster volume, (2) a short-range Coulomb potential, which corrects the latter taking into account the spatial distribution of the electron charge density of the ions; (3) an exchange term, which stems from the fact that the generalized antisymmetric product of the cluster and the external ion wave functions fulfill the first-principles requirement of antisymmetry with respect to interchange of electrons between cluster and host, and (4) a total-ion projection term, which prevents the cluster wave function from becoming linearly dependent with the host wave function;[24] this term actually prevents variational collapse of the cluster wave function on the host ions. The total-ion potentials were obtained in a self-consistent embedded-ions Hartree–Fock calculation[12] on a Cs_2ZrCl_6 (O_h^5-F_{m3m}) lattice with $a = 10.407$ Å, $x_{\mathrm{Cl}} = 0.235$.[25] The actual AIMP representation of the Cs_2ZrCl_6 host used in the embedded $(PaCl_6)^{2-}$ calculations corresponds to a μ summation in Eq. (1) made of 420 ions, which surround the $(PaCl_6)^{2-}$ cluster and are located at experimental sites within a cube of length 20.814 Å, represented by total-ion potentials, plus 2394 other ions around this cube which are represented by point charges; fractional charges were used for those in the edges so that the whole set of ions was neutral and the convergence of the Madelung potential faster.[26]

B. The $(PaCl_6)^{2-}$ defect cluster

Relativistic Cowan–Griffin–Wood–Boring[16,17]-based core AIMPs were used for both Pa ([Xe, $4f$, $5d$] core)[18] and Cl ([Ne] core).[27] For Pa, we observed that whereas the $5f$ orbitals of neutral Pa $5f^3 6d^1 7s^1 - {}^6L$ obtained in Ref. 18 do not change significantly in $Pa^{4+} 5f^1 - {}^2F$, ($\langle r\rangle_{5f}$ changes from 1.42 a.u. to 1.37 a.u.), the $6d$ orbitals suffer a very large modification ($\langle r\rangle_{6d}$ changes from 3.27 a.u. in Pa-^6L to 2.36 a.u. in $Pa^{4+} - {}^2D$.) Since we are interested here in the $6d$ states of the Pa^{4+} impurity, we produced the relativistic core AIMP and spin–orbit operators of $Pa^{4+} - {}^2D$ ([Xe, $4f$, $5d$] core) and we reoptimized and spin–orbit-corrected the d ba-

TABLE I. Cs_2ZrCl_6:$(PaCl_6)^{2-}$ spectroscopic constants. R_e in Å, $\omega_{a_{1g}}$ and T_e in cm^{-1}. Experimental data from Refs. 1 and 2 are shown in square brackets.

	Without electron correlation			With Pa-5f,6d and Cl-3p electron correlation		
Spin–free Hamiltonian						
	SCF			ACPF-37		
State	R_e	$\omega_{a_{1g}}$	T_e	R_e	$\omega_{a_{1g}}$	T_e
$5f^1$-manifold						
$^2A_{2u}$ (^2F)	2.689	323	0	2.672	311	0
$^2T_{2u}$ (^2F)	2.692	323	1 251	2.675	310	1 057
$^2T_{1u}$ (^2F)	2.698	323	3 305	2.683	310	3 522
$6d^1$-manifold						
$^2T_{2g}$ (^2D)	2.671	327	23 241	2.656	305	16 743
^2E_g (^2D)	2.743	312	54 248	2.736	270	47 120
Spin–orbit Hamiltonian						
	CI(S)			sfss-ACPF-37		
State	R_e	$\omega_{a_{1g}}$	T_e	R_e	$\omega_{a_{1g}}$	T_e
$5f^1$-manifold						
Γ_{7u} [5/2(^2F)]	2.691	323	0	2.674	310 [310]	0
Γ_{8u} [5/2(^2F)]	2.696	323	1 760	2.679	310 [310]	1 837 [2 108±1]
Γ'_{7u} [7/2(^2F)]	2.690	323	5 733	2.673	310	5 709 [5 350±50]
Γ'_{8u} [7/2(^2F)]	2.696	324	7 344	2.680	310	7 464 [7 272±3]
Γ_{6u} [7/2(^2F)]	2.697	323	8 240	2.681	309	8 526 [8 173±3]
$6d^1$-manifold						
Γ_{8g} [5/2(^2D)]	2.672	326	24 495	2.657	303 [302±4]	18 083 [19 954±3]
Γ_{7g} [5/2(^2D)]	2.671	327	27 927	2.655	305	21 507 [23 000±500]
Γ'_{8g} [3/2(^2D)]	2.743	313	56 996	2.735	271	49 958 [40 000]

sis set with respect to that in Ref. 18.[28] With the new d basis set and 6d spin–orbit operator, the atomic 6d spin–orbit coupling constant, $\zeta_{6d}=\langle 6d|V^{SO}_{6d}|6d\rangle$, is 3042 cm^{-1}, identical to the Cowan–Griffin–Wood–Boring numerical one, and significantly larger than that of neutral Pa($5f^3 6d^1 7s^1\ -^6L$), 1199 cm^{-1}. This large effect is entirely due to the 6d orbital: in effect, using the 6d spin–orbit operator of Pa($5f^3 6d^1 7s^1 -^6L$) published in Ref. 18 still leads to 3042 cm^{-1} with the new d basis set and, in consequence, we used it in the present calculations. The s, p, and f blocks of the basis set were left unchanged. The resulting $(14s10p11d9f)$ primitive Gaussian valence basis set was contracted as $[6s5p5d4f]$. For Cl, a valence basis set $(7s7p)$ contracted as $[3s4p]$ was used which resulted from the minimal $(7s6p)$ basis set of Ref. 27 upon spin–orbit correction,[29] and splitting.

C. Calculations on Cs_2ZrCl_6:$(PaCl_6)^{2-}$

We performed relativistic calculations using the spin–free and the spin–orbit Hamiltonians in $(PaCl_6)^{2-}$ embedded in the AIMP representation of the Cs_2ZrCl_6 host described above. We optimized the Pa–Cl distance of the $(PaCl_6)^{2-}$ unit under O_h symmetry, R_e, in all the states of main configuration $5f^1$ and $6d^1$, and we calculated the breathing mode vibrational frequencies, $\omega_{a_{1g}}$. From the energy curves, we calculated the minimum to minimum transition energy, T_e, that can be directly compared with the experimental zero-phonon or 0–0 transition energies because the vibrational frequencies of all the states are very similar.

We performed calculations without electron correlation effects. First, spin–free relativistic SCF calculations minimizing the average energy of the $5f^1$ states and the $6d^1$ states, respectively, produced (occupied and virtual) molecular orbitals that were used in spin–free and spin–orbit configuration interaction (CI) calculations using a CI space made of the $5f^1$ and $6d^1$ configurations plus all the single excitations to the virtual space. The results are presented in Table I under the labels SCF (spin–free Hamiltonian) and CI(S) (spin–orbit Hamiltonian).

We included the electron correlation effects by means of ACPF calculations,[20] which are MRCI-SD calculations with an approximate size-consistency correction. First, we performed spin–free relativistic ACPF calculations correlating all 36 3p electrons of the Cl ligands and the unpaired electron mainly located on Pa^{4+}. They have been loaded with the above SCF orbitals. The results are presented in Fig. 2 and Table I under the label ACPF-37. The equivalent calculations with the spin–orbit Hamiltonian are very demanding. As a simpler alternative, we used here the spin–free-state-shifted spin–orbit Hamiltonian (sfss),[12,13] which results from adding to the many-electron spin–orbit Hamiltonian the term

$$\sum_{iSM_S\Gamma\gamma} \delta(iS\Gamma)|\Phi^{\mathcal{P}}(iSM_S\Gamma\gamma)\rangle\langle\Phi^{\mathcal{P}}(iSM_S\Gamma\gamma)|, \qquad (3)$$

with

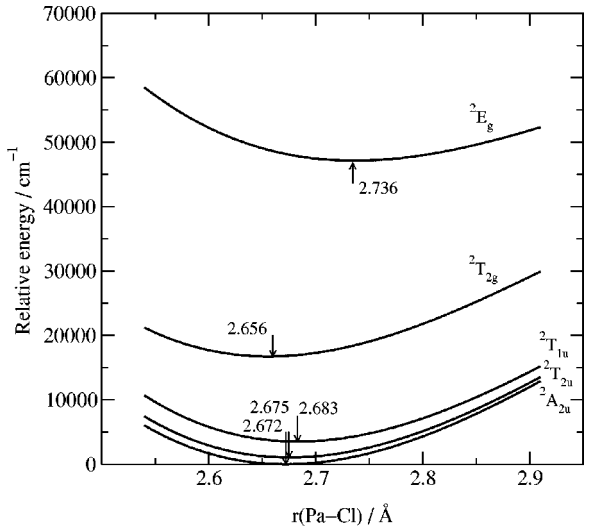

FIG. 2. Energy curves of the $5f^1$ and $6d^1$ states of Cs_2ZrCl_6:$(PaCl_6)^{2-}$ as a function of the Pa–Cl distance in the a_{1g} breathing mode. Results corresponding to the spin–free Hamiltonian including correlation effects for the 36 Cl-$3p$ electrons and the Pa open-shell electron (ACPF-37).

$$\delta(iS\Gamma)=[E^{\mathcal{G}}(iS\Gamma)-E^{\mathcal{G}}(^2A_{2u})] - [E^{\mathcal{P}}(iS\Gamma)-E^{\mathcal{P}}(^2A_{2u})]. \quad (4)$$

In Eqs. (3) and (4) $[E^{\mathcal{G}}(iS\Gamma)-E^{\mathcal{G}}(^2A_{2u})]$ are the energy differences between the spin–free states $iS\Gamma$ included in Table I ($^2T_{2u}$, $^2T_{1u}$, $^2T_{2g}$, and ^2E_g) and the $^2A_{2u}$ ground state calculated at the ACPF-37 level, $\mathcal{P}$ is a small CI space defined by the reference $5f^1$ and $6d^1$ configurations plus all the single excitations from the molecular orbitals of main character Pa-$5f$, Pa-$6d$, and Cl-$3p$ to the virtual space, and $[E^{\mathcal{P}}(iS\Gamma)-E^{\mathcal{P}}(^2A_{2u})]$ are the corresponding CI energy differences. The results are presented in Fig. 3 and Table I under the entry sfss-ACPF-37. This simple sfss Hamiltonian has been shown to be very efficient to include electron correlation effects and spin–orbit coupling effects at a time in *ab initio* calculations when they can be largely decoupled, both in transition metal elements[13–15] and lanthanide elements.[19]

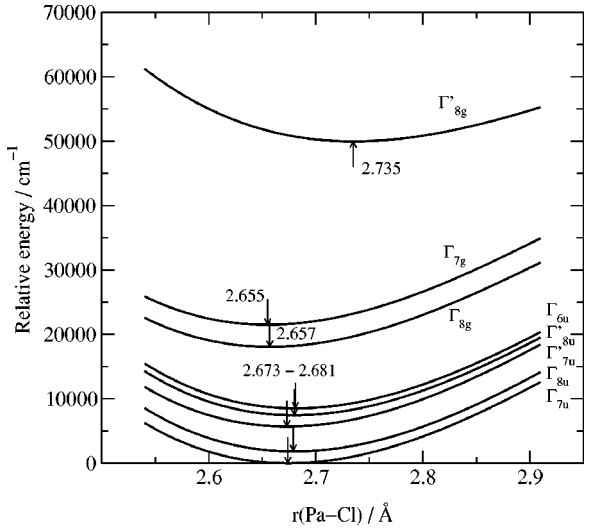

FIG. 3. Energy curves of the $5f^1$ and $6d^1$ states of Cs_2ZrCl_6:$(PaCl_6)^{2-}$ as a function of the Pa–Cl distance in the a_{1g} breathing mode. Results corresponding to the spin-dependent Hamiltonian including correlation effects for the 36 Cl-$3p$ electrons and the Pa open-shell electron (sfss-ACPF-37).

III. RESULTS

The results of the local structure of the Pa^{4+} substitutional defect in its ground- and lowest excited states are summarized in Table I; the potential energy surfaces are represented in Figs. 2 and 3. The Pa–Cl distance is in all cases larger than the host Zr–Cl distance, 2.446 Å. Lattice relaxations beyond the first coordination shell have been shown to produce negligible effects on the local distortion of the first coordination shell in related materials, such as Cr^{3+}-doped elpasolites Cs_2NaYCl_6 and Cs_2NaYBr_6,[30] and are not expected to be important here, where the $(ZrCl_6)^{2-}$ clusters are isolated. Direct measurements of these distances do not exist in this diluted material and the reliability of the theoretical results must lie on the quality of calculated distance-dependent properties and on previous calculations on similar systems. Although this is the first AIMP embedded-cluster calculation on actinide impurities, the quality of the local structures around transition metal ion impurities in ionic hosts has already been shown a number of times.[12] According to our calculations, all the states of the $5f^1$ manifold have a very similar bond distance, as expected from the internal nature of the $5f$ shell. The $6d^1$ manifold, however, shows the typical behavior of d electron states in an O_h environment: the crystal field stabilizes the $6d(t_{2g})^1$ configuration of π antibonding character with respect to the $6d(e_g)^1$ one of σ antibonding character, and the bond distance is shorter in the first case than in the second. The full balance of electrostatic and covalent interactions already considered in our most simple SCF calculations on the $(PaCl_6)^{2-}$ embedded cluster leads to slightly shorter bond distances in the $6d(t_{2g})^1$ states than in the $5f^1$ states and significantly larger bond distance in the $6d(e_g)^1$ state. The electron correlation effects due to the 36 $3p$ electrons of the Cl ligands and the open-shell electron of Pa^{4+} slightly lower, quite uniformly, all the bond distances while maintaining the qualitative picture. Finally, the spin–orbit coupling effects are of minor importance in the bond distances and only give a final touch in the definite values. The quality of the bond-distance offsets will be discussed below.

The breathing mode vibrational frequencies $\omega_{a_{1g}}$ are very slightly affected by spin–orbit coupling as well. The ligand correlation effects lowers them around 5%, except in the case of $6d^1(^2E_g)$, which is lowered 16%. The final results are in excellent agreement with the detailed experimental measurements of Refs. 1 and 2, not only in their absolute values but also in their small reduction from the $5f^1$ states (all of them essentially equal, 310 cm^{-1}) to the $6d(t_{2g})^1$ states [302 cm^{-1} in $\Gamma_{8g}[5/2(^2D)]$]. According to our results, the $6d(e_g)^1$ state ($\Gamma_{8g}[3/2(^2D)]$) shows a significantly smaller force constant ($\omega_{a_{1g}}=271\ cm^{-1}$), which has not yet been measured.

The minimum-to-minimum transition energies, T_e, calculated with and without spin–orbit and correlation effects,

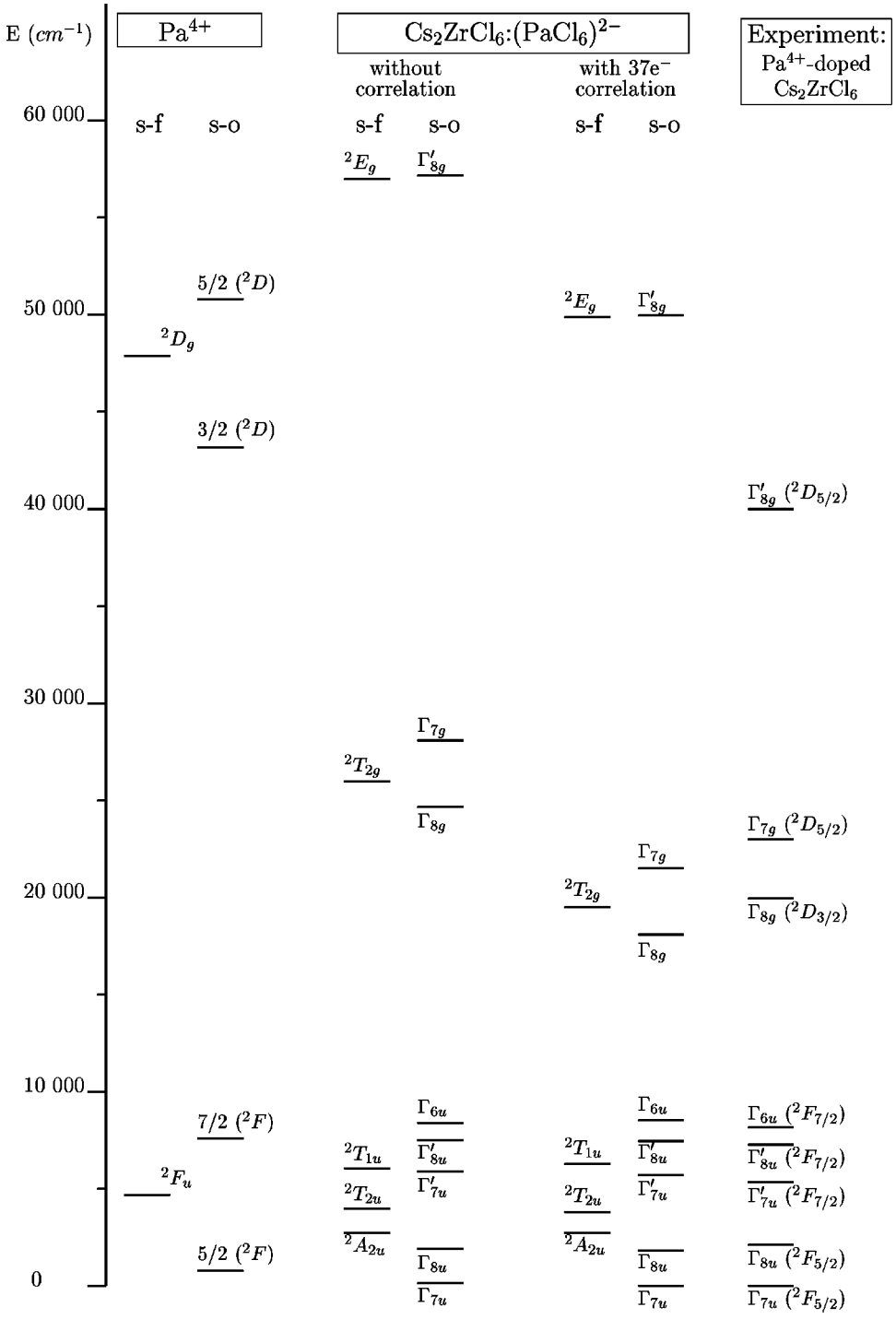

FIG. 4. $5f$ and $6d$ energy levels of Cs_2ZrCl_6:$(PaCl_6)^{2-}$. First and second columns: spin–free and spin–orbit uncorrelated calculations on the Pa^{4+} free ion. Third to sixth columns: spin–free and spin–orbit, uncorrelated and 37-electron correlated, minimum-to-minimum calculated energy differences. Last column: experimental zero-phonon energies after Piehler *et al.* (Ref. 1) and Edelstein *et al.* (Ref. 2).

are presented in Table I and Fig. 4. In order to help to understand the nature of the electronic states involved, an analysis of the spin–orbit wave functions at a given Pa–Cl distance in terms of those corresponding to a spin–free Hamiltonian are shown in Table II. Furthermore, we included in Fig. 4 the results of our calculations on the free Pa^{4+} ion: these are relativistic spin–free SCF and spin–orbit CI(S) calculations performed with the same Hamiltonian and basis set already mentioned; none of them includes electron correlation effects. A look at Fig. 4 allows one to see several effects: (i) the size of the spin–orbit coupling in free Pa^{4+} and in Cs_2ZrCl_6-embedded Pa^{4+} (both if correlation effects are absent and present); (ii) the change suffered by the $5f\rightarrow 6d$ transition when the Pa^{4+} ion is doped in the host (both if spin–orbit coupling is absent and present), which amounts to a reduction of around 9000 cm^{-1} if we compare the $^2F_u \rightarrow {}^2D_g$ free-ion transition with the energy difference between the centers of gravity of ^2E_g and $^2T_{2g}$ on the one hand and $^2T_{1u}$, $^2T_{2u}$, and $^2A_{2u}$ on the other; and (iii) the additional effect of ligand correlation on the $5f\rightarrow 6d$ transition, which is an overall reduction of the $6d^1$ manifold with respect to the $5f^1$ one.

The calculated values of T_e are compared with experimental zero-phonon levels obtained from a very detailed

TABLE II. Spectrum of Cs_2ZrCl_6:$(PaCl_6)^{2-}$ at $r(Pa–Cl)=5.100$ a.u. $=2.699$ Å, and analysis of the contributions to the spin–orbit wave functions. Energies in cm^{-1}.

State	Energy	Percentage contributions		
Γ_{7u}	0	51.57 $^2A_{2u}$	48.42 $^2T_{2u}$	0.01 residue
Γ_{8u}	1 772	57.06 $^2T_{2u}$	42.92 $^2T_{1u}$	0.02 residue
Γ'_{7u}	5 726	51.56 $^2T_{2u}$	48.43 $^2A_{2u}$	0.01 residue
Γ'_{8u}	7 395	57.06 $^2T_{1u}$	42.93 $^2T_{2u}$	0.01 residue
Γ_{6u}	8 437	99.96 $^2T_{1u}$		0.04 residue
Γ_{8g}	18 390	99.15 $^2T_{2g}$	0.81 ^2Eg	0.04 residue
Γ_{7g}	21 862	99.97 $^2T_{2g}$		0.03 residue
Γ'_{8g}	50 103	99.08 ^2Eg	0.81 $^2T_{2g}$	0.11 residue

analysis of the absorption and fluorescence spectra of Pa^{4+}-doped Cs_2ZrCl_6,[1,2] which are also included in Fig. 4. The differences in zero-point energies in the different electronic states are expected to be small enough to make such a comparison significant. It is clear that the largest effect of the (ligand) correlation included here is a lowering of the $6d$ states with respect to the $5f$ states of around $6500\,cm^{-1}$, a direct consequence of the larger extension of the $6d$ orbitals. Its effect on the $5f$ and $6d$ splittings is of minor importance. The results including correlation and spin–orbit effects show a very good agreement with the experiments in all the $5f^1$ manifold and in the $6d(\Gamma_{8g})$ and $6d(\Gamma_{7g})$ states linked to the $6d(^2T_{2g})$ state of the spin–free Hamiltonian. This excellent agreement is the result of the method under use and, in particular, of a good quality of the *ab initio* spin–orbit operators that have been employed, which, in consequence, are validated for further use. One shoud expect this good quality of the $5f$ and $6d$ Wood–Boring spin–orbit operators to stand for the rest of the actinide elements as well.

In contrast with the general good agreement between measurements and the present calculations, the disagreement in the $6d(\Gamma'_{8g})$ state of $10\,000\,cm^{-1}$ is extremely large. This state is of almost pure $6d^1-{}^2E_g$ character and mainly results from the O_h crystal field splitting of the $6d$ orbitals; accordingly, the crystal field theory (CFT) parameter $10Dq$ is essentially the energy difference between this state and the weighted average of the $6d(\Gamma_{8g})$ and $6d(\Gamma_{7g})$ of almost pure $6d^1-{}^2T_{2g}$ character. The methods and the ingredients used in this work to calculate wave functions and energies of the $(PaCl_6)^{2-}$ cluster, on one side, and to include the Cs_2ZrCl_6 host embedding effects, on the other, have been used very succesfully in a large number of transition metal impurities[12] in ionic hosts where, in particular, the precision of the O_h crystal field splittings, or $10Dq$, was always better than $1000\,cm^{-1}$, which stands as well for many other ligand field electronic transitions. Although it is true that these methods have never been applied to the calculation of $6d$ crystal field splittings, we can say that we do not find in our calculations any reason of any kind that could be considered responsible for such an unusually large deviation of $10\,000\,cm^{-1}$. In consequence with these arguments, we think that the $6d(\Gamma'_{8g})$ state of $(PaCl_6)^{2-}$ embedded in Cs_2ZrCl_6, which was first considered to be above $33\,000\,cm^{-1}$ in Ref. 1 and later observed at $40\,000\,cm^{-1}$ as a small peak preceding a small dip at approximately $42\,000\,cm^{-1}$ which is followed by a very wide absorption of the host [see Fig. 1(b) of Ref. 2] is in fact around $50\,000\,cm^{-1}$, embedded within host states. Accordingly, the CFT parameter $10Dq$ of $Pa^{4+}(6d)$ in Cs_2ZrCl_6 is larger than the presently accepted value of $18\,600\,cm^{-1}$.[2] (We calculate in fact a much larger value: $30\,000\,cm^{-1}$.) This would solve the puzzling question formulated in Ref. 2 of why the $10Dq$ of Pa^{4+}:Cs_2ZrCl_6 was smaller than the lower energy limit of $20\,000\,cm^{-1}$ given by Schwartz and Schatz[31] for the $10Dq$ of Ce^{3+}:Cs_2NaYCl_6 if the larger extension of the $6d$ orbitals would suggest a larger crystal field splitting, because the $10Dq$ of Pa^{4+}: Cs_2ZrCl_6 is larger than the $10Dq$ of Ce^{3+}: Cs_2NaYCl_6.

Let us finally comment on the bond-distance offsets of the $5f$ and $6d$ states. We can check the quality of these by calculating the band shape of the absorptions and/or emissions. In effect, the band shape is essentially controlled by the a_{1g} breathing mode offset and vibrational frequency and, since the latter is of an excellent quality, a good reproduction of the band shape would validate the former. In order to calculate the band shape we used the semiclassical time-dependent approach of Heller.[32,33] According to this, the intensity profile of an electrononic emission band reads

$$I(\omega)=C\omega^3\int_{-\infty}^{\infty}\exp(i\omega t)\langle\phi|\phi(t)\rangle dt, \tag{5}$$

where ω is the frequency of the emitted radiation, ϕ is the initial wave packet or vibrational wave function on the state origin of the emission, and $\phi(t)$ is its propagation in the final electronic state energy surface, which results from

$$i\hbar\frac{\partial\phi(t)}{\partial t}=H\phi(t)\quad(\phi(0)\equiv\phi). \tag{6}$$

If only the breathing mode is taken into account, a common value of the vibrational frequency $\omega_{a_{1g}}$ is used for the initial and final electronic states, and a harmonic approximation is assumed, the $\langle\phi|\phi(t)\rangle$ reduces to[34]

$$\langle\phi|\phi(t)\rangle=\exp\left\{-\frac{\Delta_{a_{1g}}^2}{2}(1-e^{-i\omega_{a_{1g}}t})-\frac{i\omega_{a_{1g}}t}{2}-iE_0t-\Gamma^2t^2\right\}, \tag{7}$$

where $\Delta_{a_{1g}}$ is the dimensionless a_{1g} displacement, $\Delta_{a_{1g}}=(\mu_{a_{1g}}\omega_{a_{1g}}/\hbar)^{1/2}\Delta Q_{a_{1g}}$, with $\mu_{a_{1g}}=m(Cl)$, and the breathing mode contribution to the distortion of the $(PaCl_6)^{2-}$ unit given by $\Delta R_{Pa-Cl}(a_{1g})=\Delta Q_{a_{1g}}/\sqrt{6}$, E_0 is the difference between the minima of the upper and lower energy surfaces, and Γ is an (arbitrary) damping factor whose value determines the width of the vibrational lines. The result of doing this for the fluorescence band from the lowest $6d$ state, $6d(\Gamma_{8g})$, to the lowest $5f$ state, $5f(\Gamma_{7u})$, using $\omega_{a_{1g}}=310\,cm^{-1}$ and $\Delta R_{Pa-Cl}(a_{1g})=R_e(\Gamma_{7u})-R_e(\Gamma_{8g})=0.017$ Å is presented in Fig. 5, together with the heights of the peaks in the a_{1g} sequence as extracted from Fig. 2 in Ref. 1 (shifted in energy). The agreement is excellent and, in consequence, the bond-distance offsets in the $5f$ and $6d$ states must be trusted.

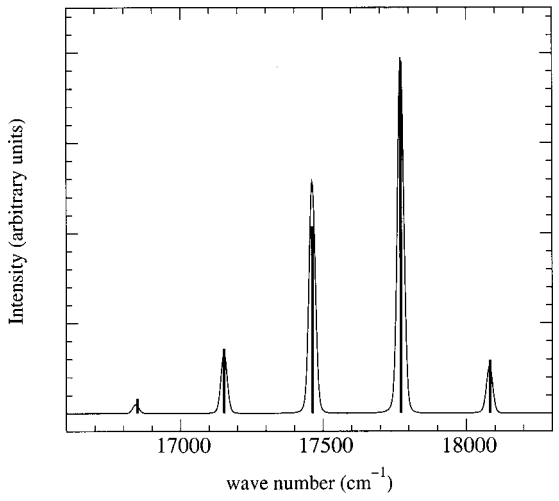

FIG. 5. Intensity profile of the emission band from the $6d(\Gamma_{8g})$ level to the $5f(\Gamma_{7u})$ level. Full line: present calculation. Vertical solid bars: Heights of the peaks in the a_{1g} sequence as extracted from Fig. 2 in Ref. 1 (shifted in energy).

IV. CONCLUSIONS

We have performed *ab initio* calculations on the $5f^1$ and $6d^1$ manifolds of the $(PaCl_6)^{2-}$ cluster embedded in a reliable representation of the Cs_2ZrCl_6 host, including embedding, electron correlation, and spin–free and spin–orbit relativistic effects. We used an AIMP embedding potential (for the first purpose) in valence ACPF calculations (for the second purpose), together with Cowan–Griffin–Wood–Boring spin–orbit relativistic AIMP core potentials (for the third purpose), in a simplified two-step procedure which decouples the treatment of correlation effects and spin–orbit coupling effects, while keeping the influence of the former on the latter.

We calculated the totally symmetric local distortions of the host induced by the Pa^{4+} impurity, both in its ground- and in its excited states, the breathing mode vibrational frequencies, and the $5f \leftrightarrow 6d$ transition energies, as well as the shape of the fluorescence band from the lowest $6d$ state to the lowest $5f$ state. The overall agreement with available experimental data is excellent and allows us to conclude, first, that the quality of the Wood–Boring AIMP spin–orbit operators used for Pa^{4+} is very high (a conclusion that may be extended to other actinide elements and which, together with the previously known quality of the spin–free components of the AIMP core potentials, supports the application of the present method to ionic hosts doped with other actinide impurities with a more complex electronic structure) and second, that both the structural and the spectroscopic information produced here are very reliable. The $6d(\Gamma'_{8g})$ state, of main character $6d(e_g)$, is not located 40 000 cm^{-1} above the ground state according to our calculations, but around 50 000 cm^{-1}. The $10Dq$ parameter of Pa^{4+} in Cs_2ZrCl_6 is 30 000 cm^{-1}. This is larger than the lower limit of 20 000 cm^{-1} accepted for Ce^{3+} in Cs_2NaYCl_6 and it would solve the problem of incompatibilities between previous $10Dq$ data for Pa^{4+} and Ce^{3+} in chloride hosts.

ACKNOWLEDGMENTS

The authors are very grateful to Professor N. Edelstein (Lawrence Berkeley Laboratory, Berkeley, California) for very helpful and supportive comments and suggestions. This work was partly supported by a grant from Ministerio de Ciencia y Tecnología, Spain (Dirección General de Investigación, No. PB98-0108).

[1] D. Piehler, W. K. Kot, and N. Edelstein, J. Chem. Phys. **94**, 942 (1991).
[2] N. Edelstein, W. K. Kot, and J. C. Krupa, J. Chem. Phys. **96**, 1 (1992).
[3] M. Karbowiak, J. Drozdzynski, S. Hubert, E. Simoni, and W. Strek, J. Chem. Phys. **108**, 10181 (1998).
[4] K. M. Murdoch, R. Cavellec, E. Simoni, M. Karbowiak, S. Hubert, M. Illemassene, and N. M. Edelstein, J. Chem. Phys. **108**, 6353 (1998).
[5] S. Matsika and R. M. Pitzer, J. Phys. Chem. A **104**, 4064 (2000).
[6] S. Matsika, R. M. Pitzer, and D. T. Reed, J. Phys. Chem. A **104**, 11983 (2000).
[7] S. Matsika and R. M. Pitzer, J. Phys. Chem. A **105**, 637 (2001).
[8] S. Matsika, Z. Shang, S. R. Brozell, J.-P. Blaudeau, Q. Wang, and R. M. Pitzer, J. Phys. Chem. A **105**, 3825 (2001).
[9] N. Edelstein, J. C. Krupa, R. C. Naik, K. Rajnak, B. Whittaker, and D. Brown, Inorg. Chem. **27**, 3186 (1988).
[10] S. Huzinaga, L. Seijo, Z. Barandiarán, and M. Klobukowski, J. Chem. Phys. **86**, 2132 (1987).
[11] Z. Barandiarán and L. Seijo, J. Chem. Phys. **89**, 5739 (1988).
[12] L. Seijo and Z. Barandiarán, in *Computational Chemistry: Reviews of Current Trends*, edited by J. Leszczynski (World Scientific, Singapore, 1999), Vol. 4, p. 55.
[13] R. Llusar, M. Casarrubios, Z. Barandiarán, and L. Seijo, J. Chem. Phys. **105**, 5321 (1996).
[14] F. Rakowitz, M. Casarrubios, L. Seijo, and C. M. Marian, J. Chem. Phys. **108**, 7980 (1998).
[15] M. Casarrubios and L. Seijo, J. Chem. Phys. **110**, 784 (1999).
[16] R. D. Cowan and D. C. Griffin, J. Opt. Soc. Am. **66**, 1010 (1976).
[17] J. H. Wood and A. M. Boring, Phys. Rev. B **18**, 2701 (1978).
[18] L. Seijo, Z. Barandiarán, and E. Harguindey, J. Chem. Phys. **114**, 118 (2001).
[19] S. Díaz-Megías and L. Seijo, Chem. Phys. Lett. **299**, 613 (1999).
[20] R. Ahlrichs, P. Scharf, and C. Ehrhardt, J. Chem. Phys. **82**, 890 (1985); R. J. Gdanitz and R. Ahlrichs, Chem. Phys. Lett. **143**, 413 (1988).
[21] L. Seijo, J. Chem. Phys. **102**, 8078 (1995).
[22] MOLCAS version 5, K. Andersson, M. Barysz, A. Bernhardsson *et al.*, Lund University, Sweden, 2000.
[23] COLUMBUS suite of programs. (ARGOS, CNVRT, SCFPQ, LSTRN, CGDBG, and CIDBG.) R. M. Pitzer (principal author). See: A. H. H. Chang and R. M. Pitzer, J. Am. Chem. Soc. **111**, 2500 (1989), and references therein for a description. CNVRT and LSTRN have been adapted to handle ECPAIMP integrals by L. Seijo. CIDBG has been modified for spin–free-state-shifted spin–orbit CI calculations by M. Casarrubios.
[24] S. Huzinaga and A. A. Cantu, J. Chem. Phys. **55**, 5543 (1971).
[25] R. W. G. Wyckoff, *Crystal Structures* (Wiley, New York, 1968).
[26] H. M. Evjen, Phys. Rev. **39**, 675 (1932).
[27] Z. Barandiarán and L. Seijo, Can. J. Chem. **70**, 409 (1992).
[28] These and other data are available from the authors upon request or directly at the address http://www.qui.uam.es/Data/AIMPLibs.html
[29] M. Casarrubios and L. Seijo, J. Mol. Struct.: THEOCHEM **426**, 59 (1998).
[30] A. Al-Abdalla, Z. Barandiarán, L. Seijo, and R. Lindh, J. Chem. Phys. **108**, 2005 (1998).
[31] R. W. Schwartz and P. N. Schatz, Phys. Rev. B **8**, 3229 (1973).
[32] E. J. Heller, J. Chem. Phys. **62**, 1544 (1975).
[33] E. J. Heller, Acc. Chem. Res. **14**, 368 (1981).
[34] J. I. Zink and K. S. Shin, *Advances in Photochemistry* (Wiley, New York, 1991), Vol. 16, pp. 119–214.